

Charge Reduction in Electrosprays: Slender Nanojets as Intermediates

Ioan Marginean, Vasilij Znamenskiy,[†] and Akos Vertes*

Department of Chemistry, Institute for Proteomics Technology and Applications,
George Washington University, Washington, DC 20052

Received: October 7, 2005; In Final Form: January 15, 2006

Molecular dynamics simulations were used to study charge reduction in electrosprayed liquids through the formation of slender nanojet intermediates. The dynamics of shape relaxation and disintegration were followed as a function of charge in cylindrical water nanojets containing protonated diglycine molecules. Depending on the overall charge, simulations showed three basic scenarios for nanojet evolution. Moderately charged nanojets reduced to spheres, whereas nanojets charged close to the Rayleigh limit divided into two offspring droplets. Due to the large Coulomb interaction between ions, highly charged nanojets suffered repeated fission until the resulting droplets were charged below the Rayleigh limit. We demonstrated the role of surface fluctuations and Maxwell stress distributions in the disintegration process. The relaxation dynamics of the moderately charged systems to spherical geometry followed a damped oscillator behavior. Compared to neutral water jets, the presence of charges in subcritical nanojets resulted in a stiffer system with longer relaxation times to spherical geometry. Interparticle forces acting between the separating offspring droplets in nanojet breakup were also determined. Due to the increased role of fluctuations in nanojets, the Rayleigh limit was shown to overestimate the maximum charge on stable systems indicating higher nanodroplet production efficiency than one would expect from macroscopic theories alone.

Small droplets are ubiquitous in the environment and are produced in many technological processes. Their formation is often associated with the instability of liquid jets. The production of droplets with microscopic dimensions (down to a few micrometers) can be conveniently followed experimentally as well as computationally.^{1,2} There are, however, limitations to the experimental exploration of nanodroplets and, especially, nanometer-size jets. Recent studies describe the behavior of neutral nanojets theoretically,³ by molecular dynamics simulations,^{4,5} or by both.⁶

Electrically charging the liquid increases the efficiency of droplet production and is currently used in fuel injection, spray painting, and inkjet printing. Electrospray ionization is one of the essential methods to transfer large biomolecular ions from solution to the gas phase.⁷ The role of jets and filaments in the electrospray process has been extensively investigated on the macroscopic scale.^{8,9} In the most studied cone-jet spraying mode, a charged liquid jet emerges from the electrified meniscus, also called Taylor cone.¹⁰ In the commonly used pulsating Taylor cone regime, standing waves on the Taylor cone induce a surface singularity that results in the ejection of a charged jet.¹¹ In time, because of escalating capillary waves this jet becomes unstable and breaks into smaller liquid columns. Depending on the amount of charge these columns hold, they may evolve to form droplets through continuous deformation or further disintegrate.

The landmark stroboscopic images of electrosprayed heptane droplets taken by Gomez and Tang indicate that the characteristic behavior observed for Taylor cones at the end of a spraying capillary, i.e., charge reduction through the formation of liquid

jets, continues on a smaller scale.¹² They observed a conical deformation of the droplets, the ejection of liquid jets from these cones, and their breakup into significantly smaller droplets. The same sequence of events is very convincingly shown on a stream of electrified microdroplets¹³ and more recently on levitated microdroplets.¹⁴

When the size of the studied system is reduced to the nanometer scale, there are experimental limitations to follow the disintegration mechanism. Apart from theoretical calculations, only molecular dynamics simulations can provide insight into the dynamics of charge reduction in nanodroplets.

In an earlier study, we applied molecular dynamics simulations to explore the structure and dynamics of nanometer-size water droplets.¹⁵ The time-averaged distribution of ions in a droplet exhibited a shell structure similar to that of Coulomb crystals observed in cold nonneutral plasmas.¹⁶ In time capillary waves developed on the initially spherical water droplets. Occasionally, the droplets became highly irregular in shape due to the formation of large surface protrusions. This behavior was especially prevalent when ions were present in the system. In critically charged systems, when such a protrusion contained an ion, the ejection of solvated ionic species followed. In their morphology (cone-jet-particle) and behavior, these extreme protrusions were similar to the Taylor cone at the electrified meniscus, and to the critically charged disintegrating microscopic droplet. A comparison of these scenarios is shown in Figure 1.

Although there is no experimental evidence for the formation of nanojets from nanodroplets, here we extend the cone-jet-particle charge reduction mechanism observed for larger systems as a hypothesis for submicron droplets. Solvent evaporation from the droplet drives the system toward a critically charged state by reducing its volume. Due to the increased curvature of the surface, this process accelerates as the droplet size decreases.

* Corresponding author. Phone: (202) 994-2717. Fax: (202) 994-5873. E-mail: vertes@gwu.edu.

[†] Current address: Department of Chemistry, City College of New York, Marshak Science Building J-1130, Convent Avenue & 138th Street, New York, NY 10030.

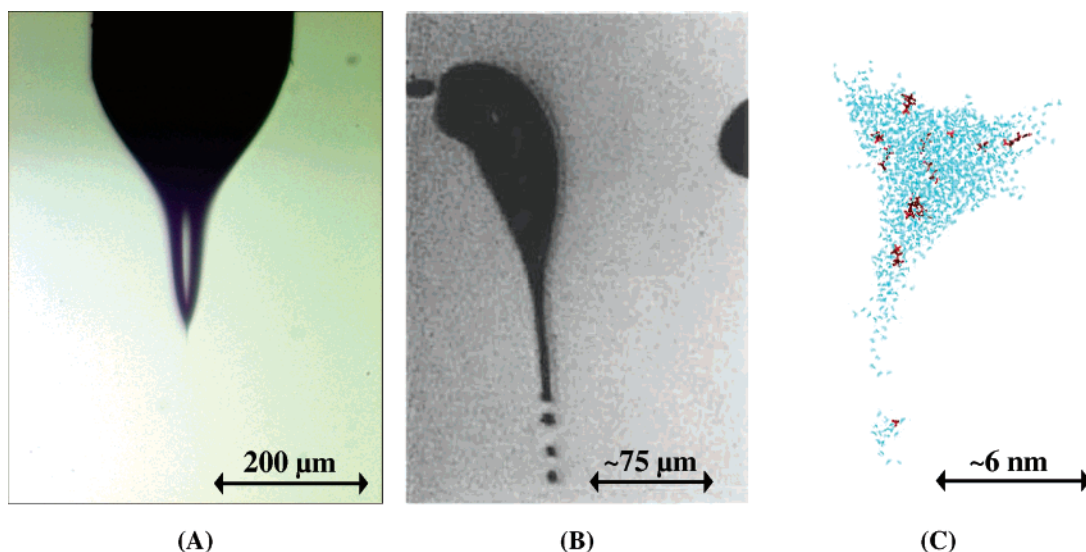


Figure 1. Morphological similarity between (A) jet ejection from a Taylor cone, (B) charge reduction of microscopic size droplets (Reprinted with permission from ref 12; Copyright 1994 American Institute of Physics), and (C) solvated ion evaporation from extreme protrusion on a nanodroplet. In all three cases, droplet formation proceeds through a jet-like protrusion from the bulk of the liquid.

We suggest that on the surface of a critically charged nanodroplet a conical protrusion is formed. In the charge reduction process a nanojet emerges from this cone that carries away a significant portion of the charge. Alternatively, a fine ligament can form at the quasisymmetric breakup of a droplet and this receding ligament can also have a jet-like geometry but with the opposite translational movement.⁸ This movement, however, does not play a role in the dynamics of deformation and can be eliminated from the calculations.

Formation of a nanojet induced by thermal and charge density fluctuations at the surface of a nanodroplet is theoretically possible. The capillary pressure fluctuation, $\Delta p_c = 2\gamma/\Delta r$, inside a protrusion induced by thermal surface fluctuations of $\Delta r = (kT/\gamma)^{1/2}$ in size can be estimated as

$$\Delta p_c = 2\sqrt{\frac{\gamma^3}{kT}} \quad (1)$$

where γ is the surface tension of the liquid at T temperature. For water at 300 K this pressure corresponds to 580 MPa. In a neutral droplet, this pressure is sufficient to eliminate the protrusion by squeezing the liquid back into the droplet where the capillary pressure is only $p_c = 2\gamma/r$, i.e., 14 MPa for a 10 nm radius droplet. Indeed, in earlier molecular dynamics calculations, 500 MPa pressure was necessary to produce neutral nanojets of propane from a 6 nm diameter nonwetting capillary.⁶

In a charged droplet, the Maxwell stress, $p_M = \epsilon_0 E^2/2$, driven by the electric field strength, E , at the cusp of the protrusion can exceed the capillary pressure and result in the formation of a jet. Here ϵ_0 stands for the electrical permittivity of vacuum. Indeed, concentrating all the $q = ze$ charges in the center, the Maxwell stress on the surface of a droplet becomes $p_M = (ze)^2/(32\pi^2\epsilon_0 r^4)$. According to Rayleigh, the number of charges, z , in critically charged droplets is

$$z^2 = 64\pi^2\epsilon_0\gamma r^3/e^2 \quad (2)$$

thus for this simplified case $p_M = 2\gamma/r$. In this basic model, at the surface of a critically charged droplet $p_M = p_c$. Charge density fluctuations, however, have a much more dramatic effect on the Maxwell stress, $p_M \propto r^{-4}$, than surface fluctuations do on the capillary pressure, $p_c \propto 1/r$.

Similarly, for jet-shaped nanoscale systems, thermal and charge density fluctuations become important and may decide the evolution of the system. For example, a surface fluctuation that increases the diameter of the nanojet adds a radial component to the velocity of molecular layers underneath. A fluctuation that decreases the nanojet diameter slows down the motion of molecules on one side and accelerates it on the other side of the fluctuation, ultimately leading to pinch-off.³ In a liquid with density ρ for the length of the pinched off segments, l_R , in neutral macroscopic jets Rayleigh's classic work predicts $l_R \approx 4.508 \times 2r$ (i.e., the wavelength of the fastest growing capillary waves) and the time it takes until pinch-off occurs, t_R , is $(r^3\rho/\gamma)^{1/2}$.¹⁷ This result is based on perturbation theory and for a jet with 1 mm radius it predicts a pinch-off time of 4 ms.

The dynamic behavior of electrified liquid bodies is significantly influenced by three physical parameters. The first two, the charge carried by the object and the surface tension, are thoroughly explored in the literature. The third parameter has to do with the morphology of the liquid. Although the lowest energy state is associated with the spherical geometry, under nonequilibrium and stationary flow conditions (e.g., liquid jets) and for certain boundary conditions (e.g., liquid bridges¹⁸) cylindrical geometry is observed. These cylindrical liquid formations are often characterized by their slenderness, $S = l/2r$, the ratio of their length, l , and diameter, $2r$. Macroscopic solutions for the surface behavior and the stability of spherical ($S = 1$) and infinitely slender ($l \gg 2r$) systems are known from perturbation theory.¹⁹

For spheres the frequency spectrum of capillary waves takes the form of

$$\omega_n^2 = \frac{n(n-1)}{\rho r^3} \left[(n+2)\gamma - \frac{z^2 e^2}{16\pi^2 \epsilon_0 r^3} \right] \quad (3)$$

and the stability criterion is given by eq 2. For infinitely slender cylinders, the frequency spectrum of varicose waves is

$$\omega_n^2 = \frac{n(n-1)}{\rho r^3} \left[(n+1)\gamma - \frac{z^2 e^2}{2\pi^2 \epsilon_0 l^2 r} \right] \quad (4)$$

where l is the length. The criterion for stability in this case is

$$z^2 = 6\pi^2\epsilon_0\gamma l^2 r/e^2 \quad (5)$$

Detailed theoretical models have been developed for macroscopic charged slender jets where the fluid can be treated as a continuum and the role of fluctuations is negligible.⁹

The few nanojet studies discussed above are exclusively concerned with neutral systems. To explore the potential role of nanojets in droplet disintegration in electrosprays, charged systems have to be considered. The presence of charges complicates the molecular dynamic treatment of liquid jets because the Coulomb forces between ions are among the dominant interactions in the system. This results in new surface phenomena. For example, when in a previous study ions were added to a water nanodroplet we noticed a dramatic increase in surface fluctuations.¹⁵ Early results on water nanojets indicate that in negatively charged jets there is a significant increase in the tangential component of the pressure tensor and the surface tension is reduced resulting in a whipping-type instability.²⁰

Once the offspring droplets are formed they continue to separate as a consequence of Coulomb repulsion. Due to the lack of experimental data, interparticle forces acting between the offspring droplets in nanojet breakup are not well characterized. Polarization and charge rearrangement effects during this phase make it difficult to develop accurate theoretical predictions. To our knowledge, the corresponding Poisson–Boltzmann problem with the appropriate boundary conditions has not been solved. Somewhat similar systems describing the interaction of polyampholytes were described by several groups.^{21,22}

Here we report on our efforts to explore the effect of thermal surface and charge density fluctuations on jet breakup in nanoscale systems. To predict the fate of liquid nanojets as a function of the amount of charge (number of ions) it contains, molecular dynamics simulations were performed for water nanojets charged below and at their Rayleigh limit. The interaction forces of the resulting charged offspring nanodroplets were followed in time.

Methods

The results presented in this paper were obtained with methods similar to what we described in a previous publication.¹⁵ Briefly, calculations using version 24b2 of the CHARMM code²³ were performed on Sun Ultra Enterprise 4000 and SGI Origin 2000 computers and the results were visualized by using the gOpenMol package^{24,25} on SGI and PC workstations. The modeling results, i.e., the particle coordinates and trajectories, were saved every 0.1 ps for further analysis.

For the interaction potentials of the water molecules the TIP3P model was used. The accuracy of the model was verified by comparing the calculated structural (g_{O-O} radial distribution function) and dynamical (enthalpy of evaporation, self-diffusion coefficient) properties with experimental values from the literature. The CHARMM22 all-atom potential function was used for the peptides. Due to the presence of long-range Coulomb interactions, the default potential cutoff parameter was increased to exceed the physical dimensions of the system. This, in turn, drastically extended the computation time.

To generate the initial coordinates and velocities of the molecules, a preequilibrated cube containing 125 water molecules was used to create larger cubes by translating its copies along the three coordinate axes. Spherical droplets were obtained by deleting molecules beyond a specified distance from the center. To account for the dominant electrostatic repulsion in finding the initial conditions, the ions were equilibrated separately in a confined space equal in size to the droplets. This

method eliminated the effect of viscosity during this phase and resulted in significantly faster equilibration of the ionic subsystem. Once equilibrated, the ions were inserted into the water droplet. Motivated by the significance of electrospray ionization of peptides and proteins, protonated diglycine molecules were selected for this study. These ions represent a tradeoff. Due to the relatively large volume and more complex solvation of these ions, they are a more realistic model for fission processes anticipated in an electrospray than elemental cations. At the same time the computational task is kept at a manageable level. The water molecules previously occupying the same space as the ions were removed and the system was reequilibrated in a 100-step geometry optimization by using potential energy minimization.

To create a jet-like geometry, the nanodroplets were inserted in a cylindrical harmonic potential along the x -axis with a harmonic potential parameter of $0.01 \text{ \AA}^{-2} \text{ kcal/mol}$. To anneal the system, heating and equilibration were performed with velocity scaling for 100 steps (0.1 ps), while the temperature was increased from 100 K to 300 K. After another heating and equilibration stage for 20 ps at an average temperature of 300 K in the restraining potential, nanojets of 11.9 nm length with a radius of 1.1 nm were obtained. During this stage, to minimize the influence of the number of charges on the length of the resulting nanojet, we used the default CHARMM cutoff distance for electrostatic forces. The nanojets were simulated in the center of mass frame, thus they can equally represent an ejected jet and a receding ligament.

Numerous exploratory calculations were performed on smaller systems (fewer water molecules and a lower number of charges). After the repeatability and self-consistency of the calculations was confirmed, six production runs for $z = 0, 7, 9, 11, 13,$ and 15 were performed at full size. It was necessary to limit the number of production runs due the excessive computation time requirements. This was the consequence of the large number of explicitly handled internal degrees of freedom and the extended cutoff distance used to accommodate the long-range Coulomb interactions in the system. When the available computational resources mentioned above were used, these calculations took over six months to complete.

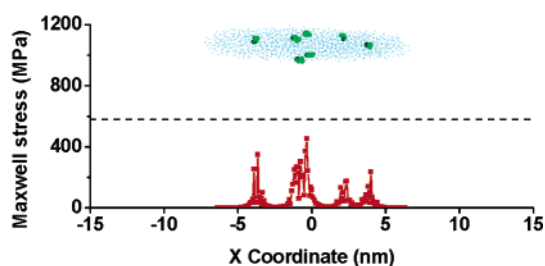
Results and Discussion

Comparing eqs 2 and 5 revealed that if a charged sphere was deformed into a slender cylinder it remained stable in a higher charge state than the sphere of the same volume if $l > 8r$ or $S > 4$. This finding is different from the stability criterion for neutral liquid bridges, where $S > \pi$ results in breakup.¹⁷ The difference stems from the boundary condition imposed at the ends of the liquid bridge. In our modeling work we focused on charged and free liquid jets of somewhat higher slenderness, $S \approx 5.2$, thus we expected these jets to be stable even if the corresponding spherical system was supercritical.

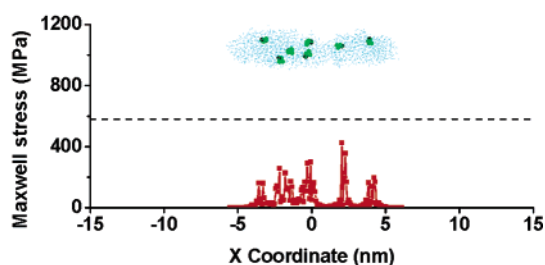
The aqueous systems we simulated consisted of ~ 1300 water molecules and $z = 0, 7, 9, 11, 13,$ and 15 diglycine ions with Rayleigh limits of 12 and 15 elementary charges for the spherical and cylindrical geometries, respectively.

Subcritical Systems. We started with the simulation of a subcritical nanojet containing 1355 water molecules and 7 diglycine ions (Figure 2). Due to dominance of the capillary pressure, the initially cylindrical system evolved toward the minimization of its exterior area. After 25 ps, close to the center of the droplet the radius of the nanojet decreased and a neck was formed, marking a possible rupture point. However, during the next 25 ps a prolate spheroidal nanodroplet was formed,

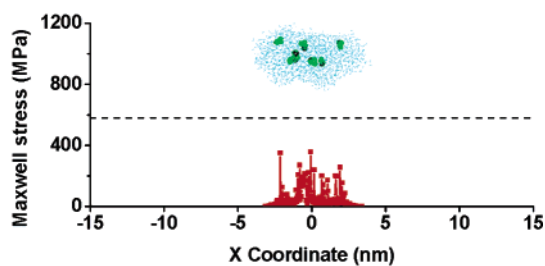
(A) 7 ions – 0 ps



(B) 7 ions – 25 ps



(C) 7 ions – 50 ps



(D) 7 ions – 75 ps

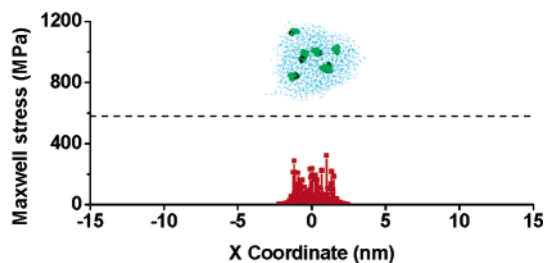
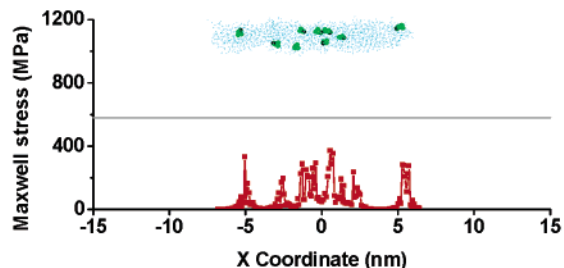


Figure 2. (A) Water nanojet containing seven diglycine ions at 0 ps evolves toward minimization of its surface, (B) after a possible breakup at 25 ps, (C) at 50 ps when the nanojet becomes elliptical, and (D) finally at 75 ps when it becomes spherical. Capillary pressure fluctuation for a neutral water droplet calculated from eq 1 equals 580 MPa, which is indicated by a dashed horizontal line throughout Figures 2–6.

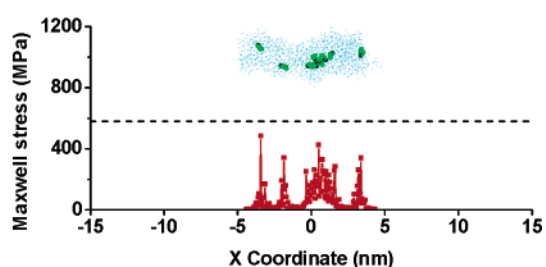
which became almost spherical after another 25 ps. We followed the slenderness as a function of time throughout the shape changes (see later). The rest of the simulation only showed changes in the shape of the droplet and thermal fluctuations on its surface. In this case the diglycine ions played a secondary role, possibly defining the position of a neck at 25 ps at the point where the charge density is minimal along the nanojet.

Figure 3 presents a few representative snapshots of the simulation that follows a system of 1324 water molecules and 9 diglycine ions. Maxwell stress distributions are also shown along the axis of the jet. As is evident in Figure 3A, the shape of the nanojet after 10 ps of evolution is still quite cylindrical. Due to the presence of ions, by 20 ps the system was highly asymmetric, with large protrusions (Figure 3B). At its peak in the 10 ps structure, the Maxwell stress remained below 390

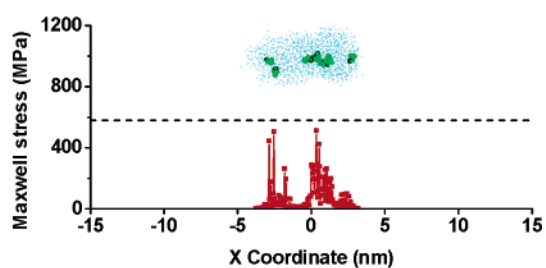
(A) 9 ions – 10 ps



(B) 9 ions – 40 ps



(C) 9 ions – 75 ps



(D) 9 ions – 130 ps

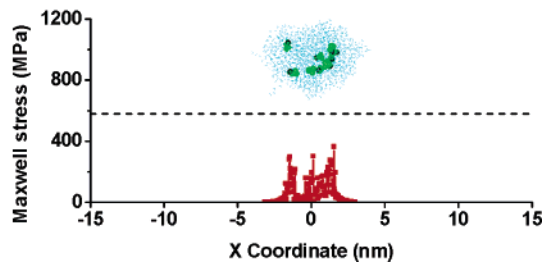


Figure 3. (A) Significant Coulomb interactions between nine diglycine ions in a subcritical jet delay formation of a spherical nanodroplet. (B) Jet keeps its slender cylindrical shape for over 40 ps, (C) by 75 ps it gradually becomes a prolate spheroid, and (D) at 130 ps it eventually assumes a spherical shape. Maxwell stress distributions along the axis of the jet show diminishing trend as a result of relaxation.

MPa. As a result of relaxation, the system progressed toward spherical shape and the maximum of the Maxwell stress distribution substantially decayed (see Figure 3D). In this simulation, no breakup of the nanojet was observed.

Compared to the lower charge states, however, the relaxation dynamics of the jet was clearly slower. After 75 ps (Figure 3C), the system was still elongated unlike the case with only 7 ions present (compare with Figure 2D). Spherical morphology of the system was only achieved after ~ 130 ps when the nanojet transformed into a nanodroplet (Figure 3D). There was no charge reduction, i.e., ion evaporation observed during the entire simulation. This finding was coherent with our previous observations, indicating that for charge densities significantly below the Rayleigh limit, ions do not evaporate from systems with slenderness $1 \leq S \leq 5.2$.¹⁵

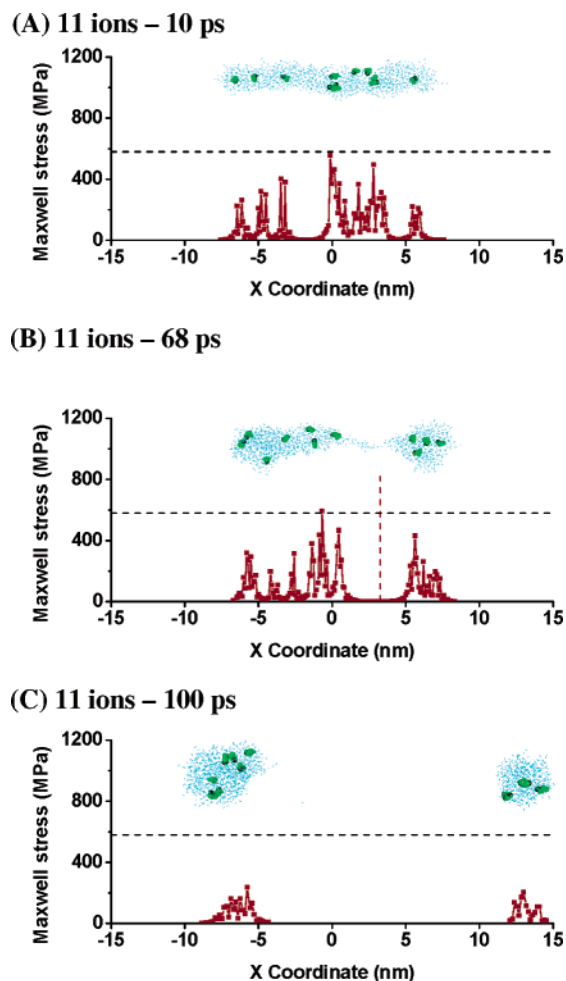


Figure 4. (A) Although still charged below the Rayleigh limit of the corresponding spherical droplet, at 10 ps the jet containing 11 diglycine ions shows elevated Maxwell stress values. (B) Due to fluctuations, jet breakup does not occur at the position with the highest Maxwell stress. At 68 ps a rupture point appears (vertical dashed line) that asymmetrically divides the jet into two fragments. (C) By 100 ps two spherical nanodroplets are formed that depart from each other.

Figure 4 presents snapshots from the simulation of a nanojet containing 1303 water molecules and 11 diglycine ions. This system represents an interesting example of a subcritical jet that ruptures due to its slenderness. The first frame (Figure 4A) shows the system at 10 ps with the surface fluctuations further increased compared to the case of only 9 ions (cf. Figure 3A). The Maxwell stress shows a sharp maximum with a value of 556 MPa. This high stress structure is the precursor of a disintegrating structure shown at ~ 68 ps in Figure 4B. Although the system was charged slightly below the Rayleigh limit of the corresponding spherical droplet ($z_R = 12$), the surface tension could not stabilize the system.

The jet breakup did not occur at the position with the highest Maxwell stress in Figure 4A. Extensive charge density fluctuations in concert with surface shape fluctuations resulted in a rupture position close to the position with the second highest Maxwell stress. Remarkably, charge partitioning into the breakup products was not symmetrical. The two offspring droplets carried 7 and 4 elementary charges, respectively, and the number of water molecules in the two droplets was proportional to their charge. It is interesting to note that the charge carried by the two spherical offspring nanodroplets formed after ~ 100 ps (Figure 4C) was below their respective Rayleigh limits.

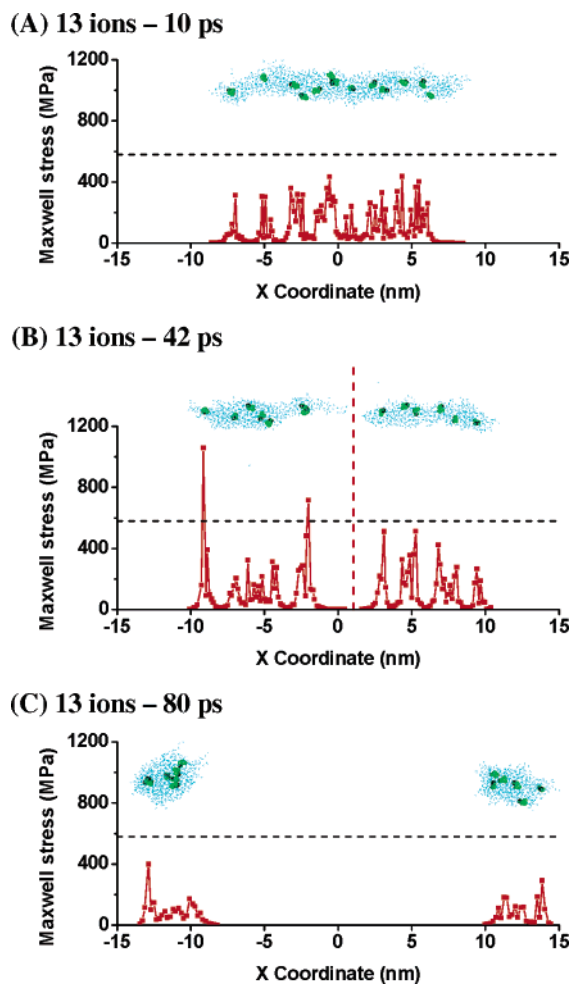


Figure 5. (A) At 10 ps, due to strong Coulomb repulsion the supercritical nanojet containing 13 diglycine ions shows kink-like instabilities. (B) The frame at 42 ps shows fast breakup (at the vertical dashed line) with very high Maxwell stress values in both fragments. (C) By 80 ps, however, the offspring droplets are stabilized through the rearrangement of charge distributions. Resulting spherical nanodroplets rapidly separate.

Supercritical Jets. Further increasing the charge to a supercharged state, i.e., to 13 diglycine ions surrounded by 1278 water molecules, resulted in the rapid disintegration of the nanojet (Figure 5). Enhanced capillary waves on the nanojet surface can be visually observed by comparing the insets in Figures 4A and 5A, but at this time stage the highest value of the Maxwell stress is comparable in the two systems. Comparing the breakup times for $z = 11$ and 13 reveals that the supercritical system ruptures at $t_b = 42$ ps (Figure 5C), i.e., 38% faster than its subcritical counterpart ($t_b = 68$ ps). In the supercritical case, the breakup was more symmetrical and the resulting spherical offspring droplets carried 6 and 7 ions, respectively, thus yielding subcritical droplets (Figure 5C). At the time of the breakup, the Maxwell stress values were very high in both fragments; however, the offspring droplets were quickly stabilized by the rearrangement of the charges.

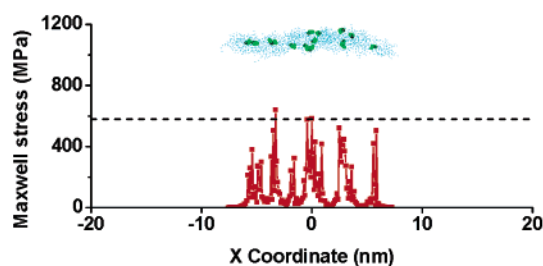
There is a remarkable similarity between the asymmetric charge distribution of the offspring droplets for $z = 11$ in the previous section and $z = 13$ above and the asymmetric charge partitioning of protein homodimers in the gas phase.²⁶ The experimental results on multiply charged Cytochrome C and reduced α -lactalbumin dimer ions indicate that the charge symmetry of the dissociation process is a strong function of the net charge on the dimer. Highly charged ions dissociate in

a symmetric fashion and produce monomers with a roughly equal number of charges, whereas dimers with a lower number of charges dissociate with highly asymmetric charge partitioning. Similarly, we found that a subcritical nanojet with 11 charges produced highly asymmetric offspring droplets with 7 and 4 charges, whereas a supercritical jet with 13 charges broke into droplets with 6 and 5 charges representing more symmetric charge partitioning. This observation may indicate a fundamental similarity between multiply charged macromolecular ions and critically charged nanojets.

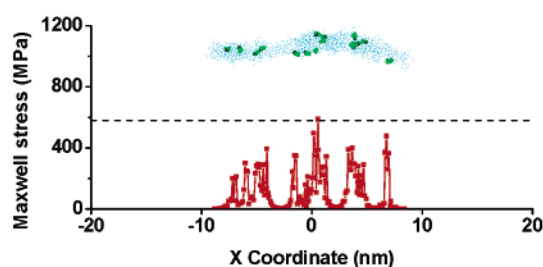
It was noticed in droplet fission experiments that during discharge events, up to 5% of the droplet mass were ejected along with 10–25% of their charge.¹ This observation implied that highly charged jets were formed. To explore this scenario, the evolution of a highly charged nanojet with 15 diglycine ions and 1256 water molecules was followed (Figure 6). Enhanced shape fluctuations were evident after 20 ps (Figure 6B), when the nanojet departed from its cylindrical shape to resemble kink instabilities. After only 36 ps (Figure 6C), the nanojet broke and another potential rupture point became visible on the larger fragment. The charge density on this offspring was still too high and after 41 ps it divided again (Figure 6D). Figure 6E presents the system after 69 ps of evolution, when three nanodroplets are already formed, each carrying a charge below or close to the Rayleigh limit. Notably, similar to our earlier observations, in Figure 6E a solvated ion evaporation event from a subcritical offspring droplet can also be identified.¹⁵ As expected, the peak values of the Maxwell stress were significantly higher in this system. After 10 ps, there were 12 points in the nanojet with 400 MPa or higher Maxwell stress values. This stress was not substantially released by the first fragmentation at 36 ps. At 69 ps, after undergoing another disintegration, the highest Maxwell stress in the three offsprings was reduced to 324 MPa. The only high stress point in the structure at that point was in the evaporating solvated ion.

Relaxation and Rupture. To follow the dynamics of shape changes in the system, we determined the average distance of molecules from the center of mass as a function of time in each nanojet. In Figure 7A, the relaxation of the original jets into spherical nanodroplets is evident for the systems containing 0, 7, and 9 diglycine ions. A damped harmonic oscillator model, $y = y_0 + A \exp(-x/\tau_{A,S \approx 5.2}) \sin(\omega x - x_c)$, gave an excellent fit of the relaxation curves with better than 0.998 regression coefficients. The obtained relaxation times were $\tau_{A,S \approx 5.2} = 20.0 \pm 1.7$ ps for $z = 7$ and $\tau_{A,S \approx 5.2} = 21.3 \pm 0.7$ ps for $z = 9$. For comparison, the relaxation of a neutral nanojet of the same dimensions was also followed. This system relaxed to spherical shape significantly faster, with $\tau_{A,S \approx 5.2} = 9.1 \pm 0.8$ ps, than the charged jets. In Table 1 these relaxation times are compared to the characteristic times of $n = 2$ capillary waves calculated from perturbation theory with eq 3 for inviscid liquid spheres ($S = 1$) and eq 4 for varicose waves on slender cylinders ($S = 5.2$). We also followed the time dependence of slenderness, $S(t)$, for the relaxing systems and used the damped oscillator model to extract characteristic times. These values are shown in the fifth column of Table 1. In all three cases, the relaxation times determined from MD calculations were between the two theoretical values. As the perturbation treatment in the theory assumes small deformations, the values for spherical systems correspond to the long time decay of the MD curve, whereas the values for cylinders are related to the initial part of the curve. The curves for the relaxing jets in Figure 7A follow the deformation of the jet from cylindrical to prolate spheroidal and finally to spherical. The intermediate geometries are not

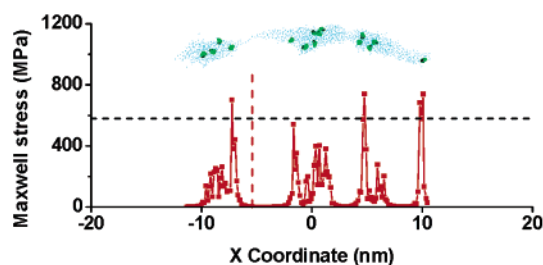
(A) 15 ions – 10 ps



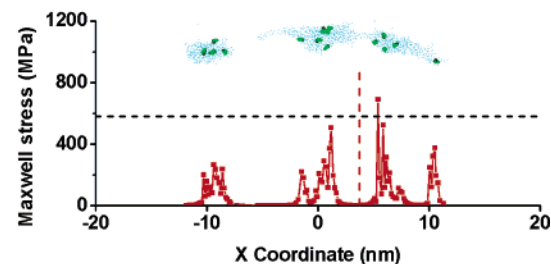
(B) 15 ions – 20 ps



(C) 15 ions – 36 ps



(D) 15 ions – 41 ps



(E) 15 ions – 69 ps

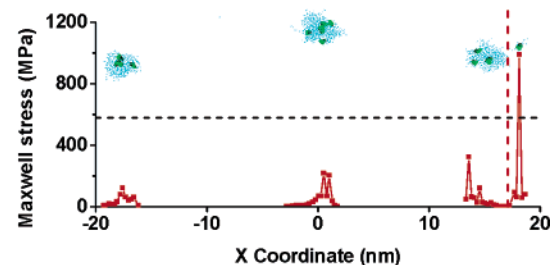


Figure 6. (A) In the case of a nanojet containing 15 diglycine ions, already at 10 ps large surface fluctuations and uniformly high Maxwell stress are present. (B) At 20 ps, bending deformations of the cylindrical jet can be observed. (C) Maxwell stress values are still high and further deformation results in two jet ruptures at 36 and (D) 41 ps. (E) After 69 ps evolution, three nanodroplets are formed each carrying a charge below or close to the Rayleigh limit. The solvated ion evaporation event from a subcritical offspring droplet can also be identified.

accessible by perturbation theory as they cannot be viewed as small deformations of either an infinitely slender cylinder or a

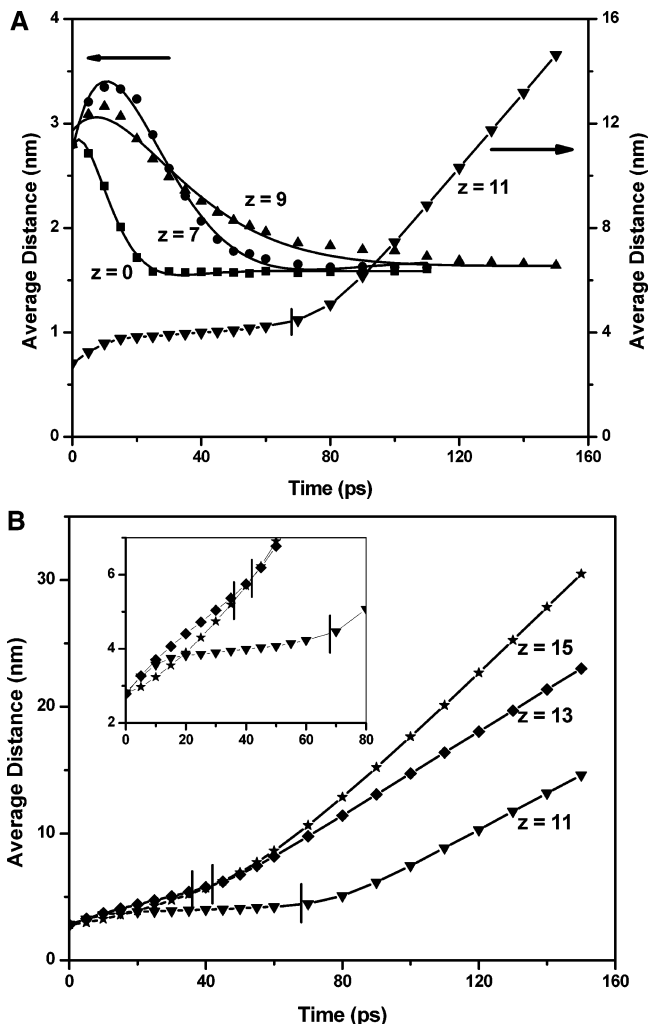


Figure 7. Dynamics of nanojet relaxation and rupture for jets of different charge is followed by the average distance of particles to the center of mass. (A) Neutral, $z = 0$ (■), and significantly subcritical jets with $z = 7$ (●) and $z = 9$ (▲) charges relax to a quasispherical state. Relaxation times increase with increasing charge from $\tau_0 = 10 \pm 2$ ps for $z = 0$ to $\tau_0 = 16 \pm 1$ ps for $z = 7$ and to $\tau_0 = 26 \pm 1$ ps for $z = 9$ charges. In contrast, a slightly subcritical (8% below the Rayleigh limit) jet with $z = 11$ (▼) breaks after $t_b = 68$ ps. (B) A comparison of rupturing jets indicates that increasing the charge on the jets results in shorter breaking times, i.e., jets with $z = 11$ (▼), 13 (◆), and 15 (★) charges rupture at $t_b = 68$, 42, and $t_b = 36$ ps, respectively.

TABLE 1: Characteristic Times for $n = 2$ Capillary Waves on Inviscid Spherical Droplets (Eq 3) and Slender Cylinders (Eq 4) from Perturbation Theory Compared to Jet Relaxation Times Obtained from the Kinetics of Average Distance, $\tau_{A,S \approx 5.2}$, and Slenderness, $\tau_{S,S \approx 5.2}$, in Molecular Dynamics Simulations

| charge state z | perturbation theory ¹⁹ | | MD simulation | |
|---------------------|-----------------------------------|---------------------|-------------------------------|-------------------------------|
| | $\tau_{S=1}$ (ps) | $\tau_{S=5.2}$ (ps) | $\tau_{A,S \approx 5.2}$ (ps) | $\tau_{S,S \approx 5.2}$ (ps) |
| 0 | 25.5 | 9.1 | 9.1 ± 0.8 | 10.5 ± 2.2 |
| 7 | 31.5 | 10.3 | 20.0 ± 1.7 | 16.5 ± 2.3 |
| 9 | 39.0 | 11.4 | 21.3 ± 0.7 | 19.4 ± 1.5 |

sphere. Indeed, following the entire process through MD is a significant new result as there is no adequate theoretical treatment that accounts for the complete dynamics of large deformations required to transform an $S = 5.2$ cylinder to a sphere. We also found that the presence of ions significantly slowed the shape relaxation process by effectively making the system stiffer.

Although the $z = 11$ subcritical droplet does not relax to spherical shape it is also represented in Figure 7A. After 68 ps of shape and charge density fluctuations a breakup of the droplet was observed at the position indicated by the vertical bar in the figure. This was a surprising finding as perturbation theory predicted charged jets of $S > 4$ to be more stable than the corresponding spherical droplet. The lower stability was attributed to the nanoscopic nature of the jet. Approaching the nanometer dimensions results in an enhanced role of surface and charge density fluctuations, an effect clearly negligible for macroscopic systems.

Figure 7B compares the behavior of the three disintegrating nanojets. The jet breakup is reflected by an increase in the slope of the average distance curves. Due to the departure of fragments at rupture, the slower but steady increase in the distance to the center of mass gives rise to a more rapid growth. The time it takes for a nanojet to break up decreases with increasing charge. Jets with $z = 11, 13,$ and 15 charges rupture at $t_b = 68, 42,$ and 36 ps, respectively.

Velocities, accelerations and forces between offspring droplets can be calculated from their displacements in time. The forces derived this way from the droplet dynamics increase with the number of charges in the nanojet, i.e., $53 \pm 5, 68 \pm 4,$ and 100 ± 13 pN for 11, 13, and 15 charges, respectively. It is interesting to compare these forces to those involved in the hydronium and diglycine ion evaporation processes described in our previous report.¹⁵ In those cases single charges were driven away from critically charged droplets by forces of 2.5 ± 0.4 and 4.5 ± 0.5 pN, respectively. This difference reveals that the slender geometry of the nanojets compared to spherical nanodroplets results in significantly larger net force fluctuations and consequently in the separation of larger segments of the original liquid body.

On the basis of data in ref 15 and in this study, we also noticed a large difference between the evaporation rate of small hydronium ions and the protonated diglycine species. In all of the simulations (droplets and jets), we observed that, in the presence of both types of ions, ion evaporation from a critically charged system invariably started with the departure of hydronium ions. Due to the increased interaction between the solvation shell of a peptide and the rest of the droplet, a further increase in the size of the ionic species would make it even more difficult for an evaporation event to take place. These observations are coherent with experiments indicating that in electrosprays small ions are produced by solvated ion evaporation, whereas large ions are formed via the charge residue mechanism.^{27,28}

It is evident from experimental data that jets are formed from unstable macroscopic droplets.^{12,14} The findings in this report suggest that if nanojets participate in the charge reduction mechanism of submicron droplets electrostatic spraying is more efficient than one would expect from the macroscopic theories alone. This enhancement is due to the reduced stability of subcritically charged slender nanojets observed in our simulations. The effect becomes increasingly significant as the dimensions of the jet are more and more reduced. As efficient ion formation is expected to happen from droplets smaller than ~ 20 nm, the reduced stability of nanojets may also have direct significance for electrospray ionization.

Acknowledgment. Helpful discussions with A. Bencsura (Chemical Research Center of the Hungarian Academy of Sciences, Hungary) regarding the use of the CHARMM code are acknowledged. This material is based upon work supported by the National Science Foundation under Grant No. 0415521,

the Department of Energy (DE-FG02-01ER15129), and the Research Enhancement Funds of George Washington University. Any opinions, findings, and conclusions or recommendations expressed in this material are those of the author(s) and do not necessarily reflect the views of the National Science Foundation or the Department of Energy.

References and Notes

- (1) Smith, J. N.; Flagan, R. C.; Beauchamp, J. L. *J. Phys. Chem. A* **2002**, *106*, 9957–9967.
- (2) Chen, A. U.; Notz, P. K.; Basaran, O. A. *Phys. Rev. Lett.* **2002**, *86*, 174501.
- (3) Eggers, J. *Phys. Rev. Lett.* **2002**, *89*, 084502.
- (4) Goto, M.; Zhigilei, L. V.; Hogley, J.; Kishimoto, M.; Garrison, B. J.; Fukumara, H. *J. Appl. Phys.* **2001**, *90*, 4755–4760.
- (5) Fang, T. H.; Chang, W. J.; Liao, S. C. *Microelectron. J.* **2004**, *35*, 687–691.
- (6) Moseler, M.; Landman, U. *Science* **2000**, *289*, 1165–1169.
- (7) Fenn, J. B.; Mann, M.; Meng, C. K.; Wong, S. F.; Whitehouse, C. M. *Science* **1989**, *246*, 64–71.
- (8) Hartman, R. P. A.; Brunner, D. J.; Camelot, D. M. A.; Marijnissen, J. C. M.; Scarlett, B. *J. Aerosol Sci.* **2000**, *31*, 65–95.
- (9) Lopez-Herrera, J. M.; Ganan-Calvo, A. M. *J. Fluid Mech.* **2004**, *501*, 303–326.
- (10) Taylor, G. *Proc. R. Soc. London A* **1964**, *280*, 383–397.
- (11) Marginean, I.; Parvin, L.; Heffernan, L.; Vertes, A. *Anal. Chem.* **2004**, *76*, 4202–4207.
- (12) Gomez, A.; Tang, K. *Phys. Fluids* **1994**, *6*, 404–414.
- (13) Hager, D. B.; Dovichi, N. J.; Klassen, J.; Kebarle, P. *Anal. Chem.* **1994**, *66*, 3944–3949.
- (14) Duft, D.; Achtzehn, T.; Müller, R.; Huber, B. A.; Leisner, T. *Nature* **2003**, *421*, 128.
- (15) Znamenskiy, V.; Marginean, I.; Vertes, A. *J. Phys. Chem. B* **2003**, *107*, 7406–7412.
- (16) Rafac, R.; Schiffer, J. P.; Hangst, J. S.; Dubin, D. H. E.; Wales, D. J. *Proc. Natl. Acad. Sci. U.S.A.* **1991**, *88*, 483–486.
- (17) Rayleigh, Lord, J. W. S. *Proc. R. Soc. London* **1879**, *29*, 71–97.
- (18) Marr-Lyon, M. J.; Thiessen, D. B.; Marston P. L. *Phys. Rev. Lett.* **2001**, *86*, 2293–2296.
- (19) Rayleigh, Lord, J. W. S. *Philos. Mag.* **1882**, *14*, 184–186.
- (20) Funakawa, T.; Yamaguchi, M.; Kumamaru, H.; Balachandran, W.; Huneiti, Z. *ILASS-Europe 2002*; Zaragoza, Spain, September 9–11, 2002.
- (21) Dobrynin, A. V.; Obukhov, S. P.; Rubinstein, M. *Macromolecules* **1999**, *32*, 5689–5700.
- (22) Tanaka, M.; Tanaka, T. *Phys. Rev. E* **2000**, *62*, 3803–3816.
- (23) MacKerell, A. D., Jr.; Bashford, D.; Bellott, M.; Dunbrack, R. L., Jr.; Evanseck, J. D.; Field, M. J.; Fischer, S.; Gao, J.; Guo, H.; Ha, S.; Joseph-McCarthy, D.; Kuchnir, L.; Kuczera, K.; Lau, F. T. K.; Mattos, C.; Michnick, S.; Ngo, T.; Nguyen, D. T.; Prodhom, B.; Reiher, W. E., III; Roux, B.; Schlenkrich, M.; Smith, J. C.; Stote, R.; Straub, J.; Watanabe, M.; Wiórkiewicz-Kuczera, J.; Yin, D.; Karplus, M. *J. Phys. Chem. B* **1998**, *102*, 3586–3616.
- (24) Laaksonen, L. *J. Mol. Graph.* **1992**, *10*, 33–34.
- (25) Bergman, D. L.; Laaksonen, L.; Laaksonen, A. *J. Mol. Graphics Modell.* **1997**, *15*, 301–306.
- (26) Jurchen, J. C.; Williams, E. R. *J. Am. Chem. Soc.* **2003**, *125*, 2817–2826.
- (27) Gamero-Castano M.; Fernandez de la Mora, J. *J. Mass Spectrom.* **2000**, *35*, 790–803.
- (28) Fernandez de la Mora, J. *Anal. Chim. Acta* **2000**, *406*, 93–104.